2

ISAR Signal Formation and Image Reconstruction as Complex Spatial Transforms

Andon Lazarov
Burgas Free University
Bulgaria

1. Introduction

Inverse aperture synthesis in the radar theory is a recording of the complex reflective pattern (complex microwave hologram) of a moving target as a complex signal. The trajectory of moving target limited by the radar's antenna pattern or time of observation is referred to as inverse synthetic aperture, and radar using the principle of inverse aperture synthesis is inverse synthetic aperture radar (ISAR). The spatial distribution of the reflectivity function of the target referred to as a target image can be retrieved from the received complex signals by applying image reconstruction techniques.

Conventional ISAR systems are coherent radars. In case the radars utilize a range-Doppler principle to obtain the desired image the range resolution of the radar image is directly related to the bandwidth of the transmitted radar signal, and the cross-range resolution is obtained from the Doppler frequency gradient generated by the radial displacement of the object relative to the radar.

A common approach in ISAR technique is division of the arbitrary movement of the target into radial displacement of its mass centre and rational motion over the mass centre. Radial displacement is compensated considered as not informative and only rotational motion is used for signal processing and image reconstruction. In this case the feature extraction is decomposed into motion compensation and image reconstruction (Li et al., 2001). Multiple ISAR image reconstruction techniques have been created, which can be divided into parametric and nonparametric methods in accordance with the signal model description and the methods of a target features extraction. (Berizzi et al., 2002; Mrtorella et al., 2003; Berizzi et al., 2004). The range-Doppler is the simplest non parametric technique implemented by two-dimensional inverse Fourier transform (2-D IFT). Due to significant change of the effective rotation vector or large aspect angle variation during integration time the image becomes blurred, then motion compensation is applied, which consist in coarse range alignment and fine phase correction, called autofocus algorithm. It is performed via tracking and polynomial approximation of signal history from a dominant or well isolated point scatterer on the target (Chen & Andrews, 1980), referred to as dominant scatterer algorithm or prominent point processing, a synthesized scatterer such as the centroid of multiple scatterers (Wu et al., 1995), referred to as multiple scatterer algorithm. Autofocus technique for random translational motion compensation based on definition of an entropy image cost function is developed in (Xi et al., 1999). Time window technique for suitable

selection of the signals to be coherently processed and to provide a focused image is suggested in (Martorella& Berizzi, 2005). A robust autofocus algorithm based on a flexible parametric signal model for motion estimation and feature extraction in ISAR imaging of moving targets via minimizing a nonlinear least squares cost function is proposed in (Li et al., 2001). Joint time-frequency transform for radar range-Doppler imaging and ISAR motion compensation via adaptive joint time-frequency technique is presented in (Chen & Qian, 1998; Qian &, Chen 1998).

In the present chapter assuming the target to be imaged is an assembly of generic point scatterers an ISAR concept, comprising three-dimensional (3-D) geometry and kinematics, short monochromatic, linear frequency modulated (LFM) and phase code modulated (PCM) signals, and target imaging algorithms is thoroughly considered. Based on the functional analysis an original interpretation of the mathematical descriptions of ISAR signal formation and image reconstruction, as a direct and inverse spatial transform, respectively is suggested. It is proven that the Doppler frequency of a particular generic point is congruent with its space coordinate at the moment of imaging. In this sense the ISAR image reconstruction in its essence is a technique of total radial motion compensation of a moving target. Without resort to the signal history of a dominant point scatterer a motion compensation of higher algorithm based on image entropy minimization is created.

2. ISAR complex signal of a point target (scatterer)

2.1 Kinematic equation of a moving point target

The Doppler frequency induced by the radial displacement of the target with respect to the point of observation is a major characteristic in ISAR imaging. It requires analysis of the kinematics and signal reflected by moving target. Consider an ISAR placed in the origin of the coordinate system (Oxy) and the point **A** as an initial position with vector **R**(0) at the moment $t = 0$, and the point **B** as a current or final position with vector **R**(t) at the moment t (Fig. 1).

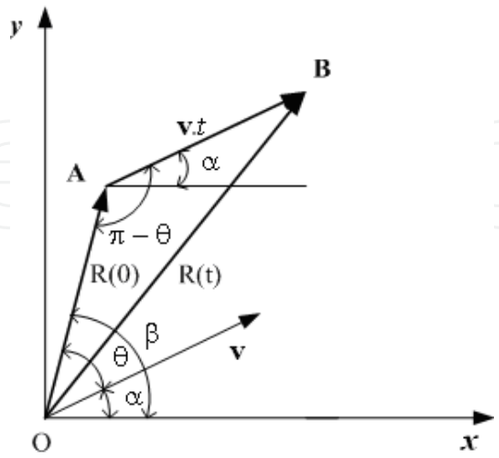

Fig. 1. Kinematics of a point target.

Assume a point target is moving at a vector velocity **v**, and then the kinematic vector equation can be expressed as

$$\mathbf{R}(t) = \mathbf{R}(0) + \mathbf{v}.t \tag{1}$$

which in matrix form can be rewritten as

$$\begin{bmatrix} x(t) \\ y(t) \end{bmatrix} = \begin{bmatrix} x(0) \\ y(0) \end{bmatrix} + \begin{bmatrix} v_x \\ v_y \end{bmatrix}.t \tag{2}$$

where $x(0) = R(0).\cos\beta$, $y(0) = R(0).\sin\beta$ are the coordinates of the initial position of the target (point **A**); $R(0) = \sqrt{x^2(0) + y^2(0)}$ is the module of the initial vector; β is the initial aspect angle; $v_x = v.\cos\alpha$, $v_y = v.\sin\alpha$ are the coordinates of the vector velocity; v is the module of the vector velocity and α is the angle between vector velocity and *Ox* axis.

The time dependent distance ISAR – point target can be expressed as

$$R(t) = \sqrt{R^2(0) + (v.t)^2 + 2(\mathbf{R}(0).\mathbf{v}).t}\ , \tag{3}$$

where $\mathbf{R}(0).\mathbf{v}$ is the inner product, defined by $\mathbf{R}(0).\mathbf{v} = x(0)v_x + y(0)v_y$ or $\mathbf{R}(0).\mathbf{v} = R(0).v.\cos\theta$; $\theta = \beta - \alpha$ is the angle between position vector $\mathbf{R}(0)$ and vector velocity $\mathbf{v}$, defined by the equation

$$\theta = \arccos\frac{x(0).v_x + y(t).v_y}{R(0).v}\ . \tag{4}$$

Then Eq. (3) can be rewritten as

$$R(t) = \sqrt{R^2(0) + (v.t)^2 + 2R(0)(v.t)\cos\theta}\ , \tag{5}$$

where $R(0)$ is the distance to the target at the moment $t = 0$, measured on *OA*, the initial line of sight (LOS).

The radial velocity of the target at the moment *t* is defined by differentiation of Eq. (5), i.e.

$$v_r(t) = \frac{dR(t)}{dt} = \frac{v^2 t + R(0).v.\cos\theta}{\sqrt{R^2(0) + (v.t)^2 + 2R(0).v.t.\cos\theta}}\ . \tag{6}$$

If $t = 0$, the radial velocity $v_r(0) = v\cos\theta$. In case the angle θ = 0, then $v_r(0) = v$. At the moment $t = T$ when $v.T = -R(0)\cos\theta$ the target is on the traverse, then $v_r(T) = 0$, and $T = \frac{-R(0)\cos\theta}{v}$, which for the kinematics in Fig. 1 requires an angle θ to have a value $\theta \geq \pi/2$. The time variation of the radial velocity of the target causes a time dependent Doppler shift in the frequency of the signal reflected from the target.

2.2 Doppler frequency of a moving point target

Assume that the ISAR emits to the target a continuous sinusoidal waveform, i.e.

$$s(t) = A_0 \exp(j\omega t), \tag{7}$$

where A_0 is the amplitude of the emitted waveform, $\omega = 2\pi f = \frac{2\pi.c}{\lambda}$ is the angular frequency, f is the carrier frequency, λ is the wavelength of the emitted waveform, $c = 3.10^8$ m/s is the speed of the light in vacuum.

The signal reflected from the target can be defined as a time delayed replica of the emitted waveform, i.e.

$$s(t) = A_i \exp(j\omega(t - t_i)) \tag{8}$$

where A_i is the amplitude of the reflected signal, $t_i = \frac{2R_i(t)}{c}$ is the time delay of the replica of the emitted waveform, $R_i(t)$ is the radial slant range distance to the target, calculated by Eq. (5). Define the general phase of the reflected signal as

$$\Phi(t) = \omega\left(t - \frac{2R_i(t)}{c}\right). \tag{9}$$

Then the current angular frequency of the reflected signal can be determined as

$$\hat{\omega}(t) = \frac{d\Phi(t)}{dt} = \omega - 2\frac{\omega}{c}.\frac{dR_i(t)}{dt}, \tag{10}$$

$$\hat{\omega}(t) = \frac{d\Phi(t)}{dt} = \omega - \frac{4\pi}{\lambda}.\frac{dR_i(t)}{dt}, \tag{11}$$

where $\omega_D(t) = \frac{4\pi}{\lambda}.\frac{dR_i(t)}{dt}$ is the angular time dependent Doppler frequency.

For the closing target $\frac{dR_i(t)}{dt} < 0$, then the angular Doppler frequency is a negative, $\omega_D(t) < 0$, and current angular frequency of the signal reflected from the target, $\hat{\omega}(t)$, increases, i.e. $\hat{\omega}(t) = \omega + \omega_D(t)$. For a receding target $\frac{dR_i(t)}{dt} > 0$, then the angular Doppler frequency is a positive, $\omega_D(t) > 0$, and current frequency of the signal reflected from the target, $\hat{\omega}(t)$, decreases, i.e. $\hat{\omega}(t) = \omega - \omega_D(t)$.

Based on Eq. (6) the angular Doppler frequency can be expressed as

$$\omega_D(t) = \frac{4\pi}{\lambda}\frac{v^2.t + R(0).v.\cos\theta}{\sqrt{R^2(0) + (v.t)^2 + 2R(0).v.t\cos\theta}}. \tag{12}$$

Accordingly the absolute Doppler frequency can be defined as

$$F_D(t) = \frac{2}{\lambda}.\frac{v^2.t + R(0).v.\cos\theta}{\sqrt{R^2(0) + (v.t)^2 + 2R(0).v.t.\cos\theta}}. \tag{13}$$

If $t = 0$, then $F_D(0) = \frac{2}{\lambda}.v.\cos\theta$. If $\theta = 0$, then $F_D(0) = \frac{2}{\lambda}.v$. At the moment $t = T$, i.e $v.T = -R(0)\cos\theta$ the target is on the traverse, then $F_D(T) = 0$. At the particular moment t and $\theta = 0$, $F_D(t) = \frac{2}{\lambda}.v$ is constant, and for $\theta = \pi/2$, $F_D(t) = \frac{2}{\lambda}.\frac{v^2.t}{\sqrt{R^2(0) + (v.t)^2}}$. Hence in case $\theta \neq 0$ the Doppler frequency is time dependent during the aperture syntheses, coherent processing interval (CPI), but only one value has a meaning for ISAR imaging, the value defined at the moment of imaging, which will be proven in subsection 3.3.

2.3 Numerical experiments

2.3.1 Example 1

Assume that the point target is moving at the velocity v =29 m/s and illuminated by a continuous waveform with wavelength $\lambda = 3.10^{-2}$ m (frequency $f = 10^{10}$ Hz). CPI time t = 712 -722 s s, initial distance $R(0) = 10^5$ m, guiding angle $\alpha = 0.9.\pi$, position angle $\beta = \pi/3$. The calculation results of the current signal frequency and Doppler frequency are illustrated in Figs 2, (a), and (b).

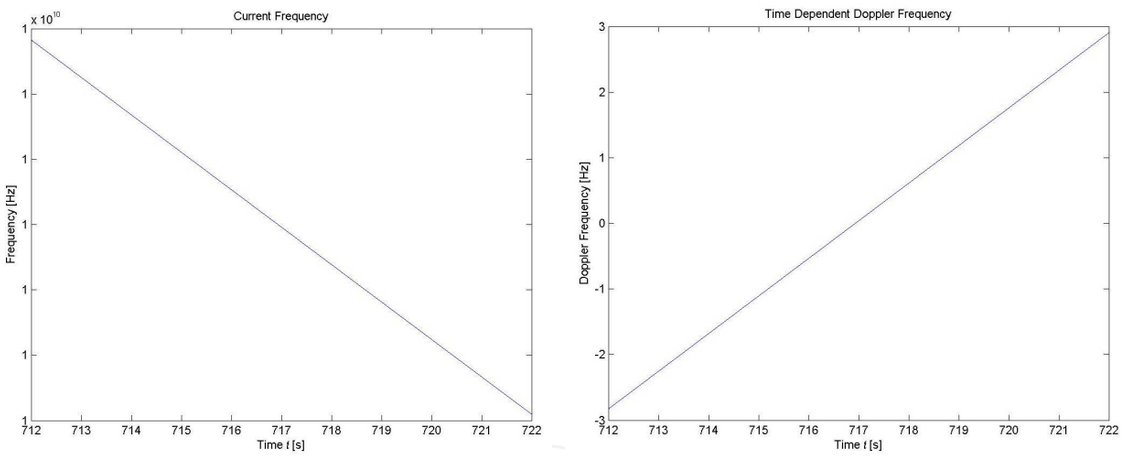

(a) Current ISAR signal frequency (b) Doppler frequency

Fig. 2. Current ISAR signal and Doppler frequency caused by time varying radial velocity.

It is worth noting that the current signal frequency decreases during CPI due to the alteration of the value and sign of the Doppler frequency varying from -3 to 3 Hz. At the moment t = 717 s the Doppler frequency is zero. The time instance where Doppler changes its sign (zero Doppler differential) can be regarded as a moment of target imaging.

Computational results of the imaginary and real part of ISAR signal reflected by a point target with time varying radial velocity are presented in Figs. 3, (a), and (b). It can be clearly seen the variation of the current frequency of the signal due to the time dependent Doppler frequency of the point target. The existence of wide bandwidth of Doppler variation in the signal allows multiple point scatterers to be potentially resolved at the moment of imaging.

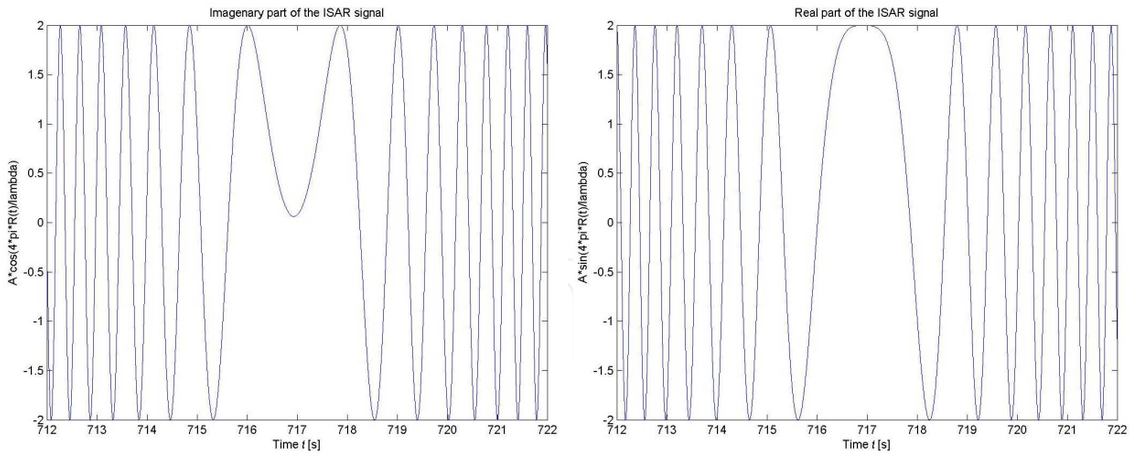

(a) Imaginary part of an ISAR signal (b) Real part of an ISAR signal.

Fig. 3. Imaginary and real part of ISAR signal reflected by a point target.

2.3.2 Example 2

It is assumed that the point target moves at the velocity v =29 m/s and is illuminated with continuous waveform with wavelength $\lambda = 10^{-2}$ m (frequency $f = 3.10^{10}$ Hz). CPI time t = 0 - 2 s, initial distance $R(0)$ = 30 m, guiding angle $\alpha = \pi$ and position angle, $\beta = 0$. The calculation results of the current signal frequency and Doppler frequency are illustrated in Figs 4, (a), and (b).

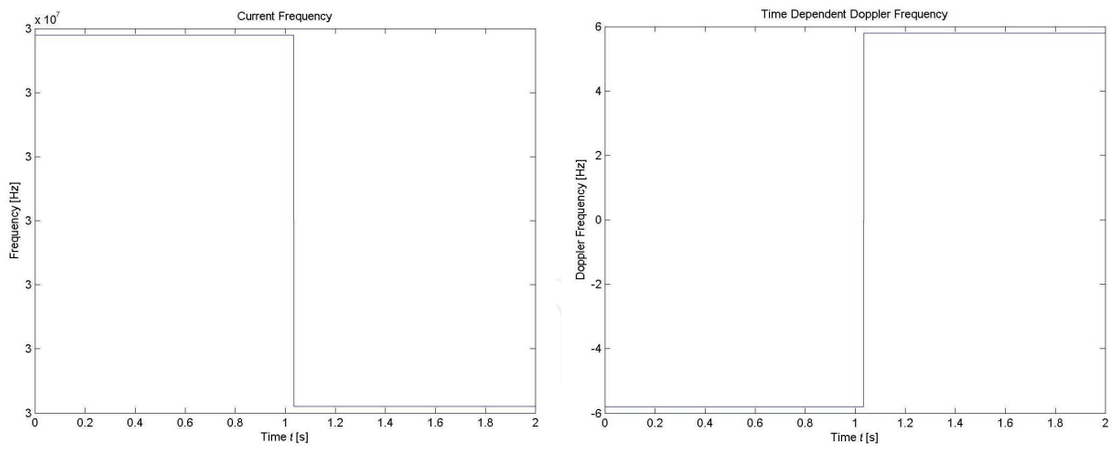

(a) Current ISAR signal frequency (b) Doppler frequency

Fig. 4. Current ISAR signal frequency and Doppler frequency with a constant radial velocity.

It can be seen that the current signal frequency has two constant values during CPI due to the constant Doppler frequency with two signs, -5.8 Hz and +5.8 Hz. At the moment t = 1.04 s the Doppler frequency alters its sign. The time instance where Doppler changes its sign (zero Doppler differential) can be regarded as a moment of point target imaging that means one point target can be resolved.

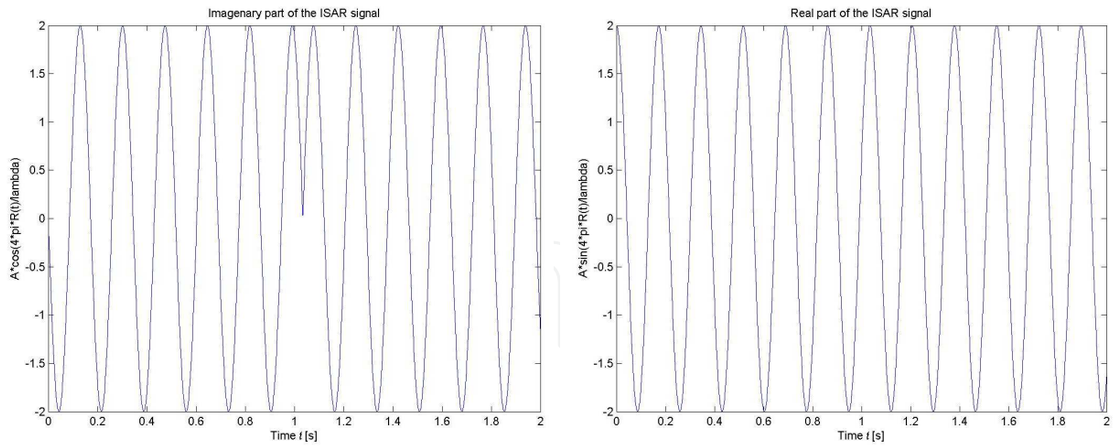

(a) Imaginary part of an ISAR signal (b) Real part of an ISAR signal.

Fig. 5. Imaginary and real part of ISAR signal reflected by a point target.

Computational results of the imaginary and real part of ISAR signal reflected by a point target with constant radial velocity are presented in Figs. 5, (a), and b. It can be clearly seen the change of the phase in the imaginary part of the ISAR signal.

3. ISAR signal formation and imaging with a sequence of monochromatic short pulses

3.1 3-D ISAR geometry and kinematics

The basic characteristic in ISAR imaging is the time dependent distance between a particular generic point from the target and ISAR. Consider 3-D geometry of ISAR scenario with radar and moving target in the coordinate system $Oxyz$ (Fig. 6). The target is located in a regular grid, defined in the coordinate system $O'XYZ$. The generic point scatterer **g** from the target area is specified by the index vector (i,j,k), i.e. $\mathbf{g}=(i,j,k)$. The position vector $\mathbf{R}_{ijk}(p)$ of the ijk th generic point scatterer in the coordinate system $Oxyz$ at the moment p is described by the following vector equation

$$\mathbf{R}_{ijk}(p)=\mathbf{R}_{00'}(0)+\mathbf{V}T_p\left(\frac{N}{2}-p\right)+\mathbf{A}\mathbf{R}_{ijk}\,, \tag{14}$$

where $\mathbf{R}_{ijk}(p)=\left[x_{ijk}(p),{y_{ijk}}^2(p),{z_{ijk}}^2(p)\right]^T$, $x_{ijk}(p),y_{ijk}(p)$, and $z_{ijk}(p)$ are the current coordinates of the generic point, T_p denotes the pulse repetition period; $p=\overline{1,N}$ denotes the index of the emitted pulse, N denotes the full number of the emitted pulses during CPI; $\mathbf{R}_{00'}(0)=\left[x_{00'}(0),y_{00'}(0),z_{00'}(0),\right]^T$ is the position vector of the target geometric center, that locates a point O' at the moment $p=\frac{N}{2}$, $\mathbf{V}=[V_x,V_y,V_z]^T$ denotes the vector velocity with coordinates $V_x=V\cos\alpha$, $V_y=V\cos\beta$ and $V_z=V\cos\delta$; $\mathbf{R}_{ijk}=[X_{ijk},Y_{ijk},Z_{ijk}]^T$ denotes the position vector of the ijk th generic point; $X_{ijk}=i(\Delta X)$, $Y_{ijk}=j(\Delta Y)$ and $Z_{ijk}=k(\Delta Z)$ denote

the discrete coordinates of the ijk th generic point in the coordinate system $O'XYZ$; ΔX, ΔY and ΔZ denote the dimensions of the grid cell; $\cos\alpha$, $\cos\beta$ and $\cos\delta = \sqrt{1-\cos^2\alpha-\cos^2\beta}$ are the guiding cosines; V is the module of the vector velocity.

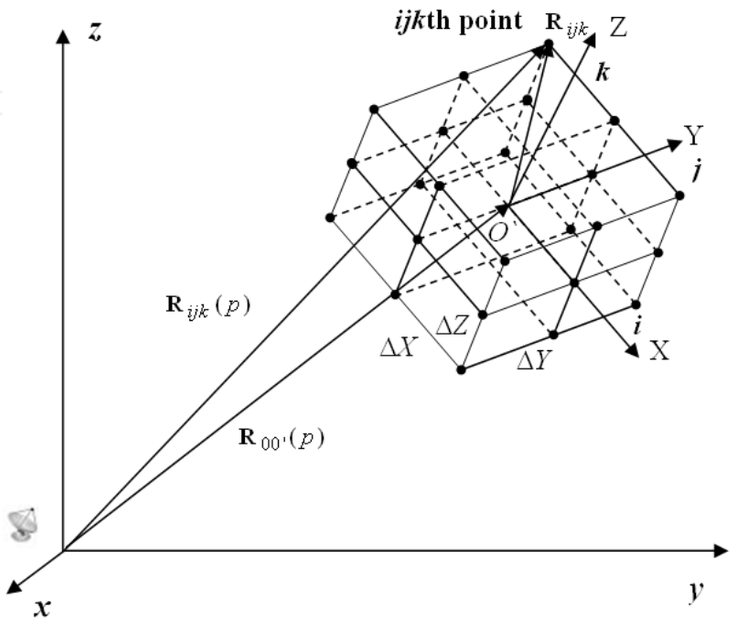

Fig. 6. Geometry of 3-D ISAR scenario.

The elements of the transformation matrix **A** in Eq. (14) are determined by the Euler expressions

$$\begin{aligned}
a_{11} &= \cos\psi\cos\varphi - \sin\psi\cos\theta\sin\varphi;\\
a_{12} &= -\cos\psi\sin\varphi - \sin\psi\cos\theta\cos\varphi;\\
a_{13} &= \sin\psi\sin\theta;\\
a_{21} &= \sin\psi\cos\varphi + \cos\psi\cos\theta\sin\varphi; \quad a_{31} = \sin\theta\sin\varphi;\\
a_{22} &= -\sin\psi\sin\varphi + \cos\psi\cos\theta\cos\varphi; \; a_{32} = \sin\theta\cos\varphi;\\
a_{23} &= -\cos\psi\sin\theta; \qquad a_{33} = \cos\theta.
\end{aligned} \tag{15}$$

The projection angles ψ, θ and φ, defining the space orientation of the 3-D grid are calculated by components A, B, C of the normal vector to the plane that specifies the position of the target, and coordinates of the vector velocity, i.e.

$$\psi = \arctan\left(-\frac{A}{B}\right); \theta = \arccos\frac{C}{[(A)^2+(B)^2+(C)^2]^{\frac{1}{2}}} \tag{16}$$

$$\varphi = \arccos\frac{V_xB - V_yA}{\{[(A)^2+(B)^2][(V_x)^2+(V_y)^2+(V_z)^2]\}^{\frac{1}{2}}}. \tag{17}$$

The components A, B, C of the normal vector are determined by the components of the position vector $\mathbf{R}_{00'}(0) = [x_{00'}(0), y_{00'}(0), z_{00'}(0),]^T$, vector velocity of the target and vector position of an arbitrary reference point $\mathbf{R}_0 = [x_0(0), y_0(0), z_0(0)]^T$ in the coordinate system $Oxyz$ by expressions

$$\begin{aligned} A &= V_z[y_{00'}(0) - y_0(0)] - V_y[z_{00'}(0) - z_0(0)]; \\ B &= V_x[z_{00'}(0) - z_0(0)] - V_z[x_{00'}(0) - x_0(0)]; \\ C &= V_y[x_{00'}(0) - x_0(0)] - V_x[y_{00'}(0) - y_0(0)]. \end{aligned} \tag{18}$$

The projection of the vector equation (14) on Cartesian coordinates yields

$$\begin{bmatrix} x_{ijk}(p) \\ y_{ijk}(p) \\ z_{ijk}(p) \end{bmatrix} = \begin{bmatrix} x_{00'}(0) + V_x\left(\frac{N}{2} - p\right).T_p \\ y_{00'}(0) + V_y.\left(\frac{N}{2} - p\right).T_p \\ z_{00'}(0) + V_z.\left(\frac{N}{2} - p\right).T_p \end{bmatrix} + \begin{bmatrix} a_{11} & a_{12} & a_{13} \\ a_{21} & a_{22} & a_{23} \\ a_{31} & a_{32} & a_{33} \end{bmatrix}.\begin{bmatrix} X_{ijk} \\ Y_{ijk} \\ Z_{ijk} \end{bmatrix}, \tag{19}$$

then the distance between the generic point and ISAR can be expressed as

$$R_{ijk}(p) = \left[{x_{ijk}}^2(p) + {y_{ijk}}^2(p) + {z_{ijk}}^2(p) \right]^{\frac{1}{2}} \tag{20}$$

Eq. (20) is used in calculation of the time delay of the signal reflected by a particular generic point scatterer from the target area while signal modeling.

3.2 Short pulse ISAR signal formation

Consider 3-D ISAR scenario (Fig. 6) and a generic point **g** from the target illuminated by sequence of short monochromatic pulses, each of which is described by

$$s(t) = A.\mathrm{rect}\left(\frac{t}{T}\right)\exp(j.\omega t), \tag{21}$$

$$\mathrm{rect}\frac{t}{T} = \begin{cases} 1, 0 \le \frac{t}{T} < 1, \\ 0, \text{ otherwise.} \end{cases}$$

where A is the amplitude of the emitted signal, $\omega = 2\pi\frac{c}{\lambda}$ is the angular frequency; $c = 3.10^8$ m/s is the speed of the light in vacuum; λ is the wavelength of the signal; T is the timewith of the emitted pulse.

The signal reflected by the generic point scatter can be written as

$$s_{\mathbf{g}}(p,t) = a_{\mathbf{g}}\,\mathrm{rect}\frac{t - t_{\mathbf{g}}(p)}{T}\exp\{j\omega[t - t_{\mathbf{g}}(p)]\}, \tag{22}$$

$$\text{rect}\frac{t-t_{\mathbf{g}}(p)}{T}=\begin{cases}1,\ 0\le\dfrac{t-t_{\mathbf{g}}(p)}{T}<1,\\ 0,\ \text{otherwise.}\end{cases}$$

where $t_{\mathbf{g}}(p)=\dfrac{2R_{\mathbf{g}}(p)}{c}$ is the time delay of the signal, $\mathbf{g}$ stands for the discrete vector coordinate that locates the generic point scatterer in the target area $\mathbf{G}$, $a_{\mathbf{g}}$ stands for the magnitude of the 3-D discrete image function, $\tilde{t}=t \bmod T_p$ is the slow time, p denotes the number of the emitted pulse, T_p is the pulse repetition period, $t=\tilde{t}-pT_p$ is the fast time, presented as $t=k.T$, where k is the number of range bin, where the ISAR signal is placed. The demodulated ISAR signal from the target area is

$$s(p,k)=\sum_{\mathbf{g}\in\mathbf{G}}a_{\mathbf{g}}\,\text{rect}\frac{k.T-t_{\mathbf{g}}(p)}{T}.\exp\{-j\omega t_{\mathbf{g}}(p)]\}\,. \tag{23}$$

The expression (23) is a weighted complex series of finite complex exponential base functions. It can be regarded as an asymmetric complex transform of the 3-D image function $a_{\mathbf{g}}$, $\mathbf{g}\in\mathbf{G}$, defined for a whole discrete target area $\mathbf{G}$ into 2-D signal plane $s(p,k)$.

3.3 Image reconstruction from a short pulse ISAR signal

Eq. (23) can be rewritten as

$$s(p,k)=\sum_{\mathbf{g}\in\mathbf{G}}a_{\mathbf{g}}.\text{rect}\frac{k.T-\dfrac{2R_{\mathbf{g}}(p)}{c}}{T}.\exp\left[-j\frac{4\pi}{\lambda}R_{\mathbf{g}}(p)\right] \tag{24}$$

Formally for each kth range cell the image function can be extracted by the inverse transform

$$\hat{a}_{\mathbf{g}}=\sum_{p=1}^{N}s(p,k)\exp\left[j\frac{4\pi}{\lambda}R_{\mathbf{g}}(p)\right] \tag{25}$$

where p is the number of emitted pulse, N is the full number of emitted pulses during CPI.

Because $s(p,k)$ is a 2-D signal, only a 2-D image function $\hat{a}_{\mathbf{g}}$ can be extracted. Eq. (25) is a symmetric complex inverse spatial transform or inverse projective operation of the 2-D signal plane $s(p,k)$ into 2-D image function $\hat{a}_{\mathbf{g}}$, and can be regarded as a spatial correlation between $s(p,k)$ and $\exp\left[j\dfrac{4\pi}{\lambda}R_{\mathbf{g}}(p)\right]$. Moreover, Eq. (25) can be interpreted as a total compensation of phases, induced by radial displacement $R_{\mathbf{g}}(p)$ of the target. Taylor expansion of the distance to the generic point, $R_{\mathbf{g}}(p)$ at the moment of imaging is

$$R_{\mathbf{g}}(p)=r_{\mathbf{g}}+v_{\mathbf{g}}(pT_p)+\frac{a_{\mathbf{g}}}{2!}(pT_p)^2+\frac{h_{\mathbf{g}}}{3!}(pT_p)^3+\ldots\,, \tag{26}$$

where $r_{\mathbf{g}}$, $v_{\mathbf{g}}$, $a_{\mathbf{g}}$ and $h_{\mathbf{g}}$ is the distance, radial velocity, acceleration and jerk of the generic point, respectively at the moment of imaging.

Due to range uncertainty of generic points placed in the kth range resolution cell, $r_{\mathbf{g}}$ can be assumed constant, and (25) can be written as

$$\hat{a}_{\mathbf{g}} = \exp\left(j\frac{4\pi}{\lambda} r_{\mathbf{g}} \right) \sum_{p=1}^{N} s(p,k) \exp\left(j\frac{4\pi}{\lambda} [v_{\mathbf{g}}(pT_p) + \frac{a_{\mathbf{g}}}{2!}(pT_p)^2 + \frac{h_{\mathbf{g}}}{3!}(pT_p)^3 + ...] \right). \tag{27}$$

Eq. (27) stands for a procedure of total motion compensation of every generic point from kth range resolution cell. The range distance $r_{\mathbf{g}}$ does not influence on the image reconstruction and can be removed from the equation (27), i.e.

$$\hat{a}_{\mathbf{g}} = \sum_{p=1}^{N} s(p,k) \exp\left(j2\pi [\frac{2}{\lambda} v_{\mathbf{g}}(pT_p) + \frac{1}{\lambda} a_{\mathbf{g}}(pT_p)^2 + \frac{1}{3} h_{\mathbf{g}}(pT_p)^3 + ...] \right). \tag{28}$$

For each kth range cell the term $\frac{2}{\lambda} v_{\mathbf{g}}$ stands for the Doppler frequency whereas terms as $\frac{2}{\lambda} a_{\mathbf{g}}$, $\frac{2}{\lambda} h_{\mathbf{g}}$ …., denote the higher order derivations of the time dependent Doppler frequency, defined at the moment of imaging.

If the Doppler frequency of generic points in the kth range cell is equal or tends to constant during CPI the equation (28) reduces to the following equation of radial motion compensation

$$\hat{a}_{\mathbf{g}} = \sum_{p=1}^{N} s(p,k) \exp\left(j2\pi . \left(\frac{2}{\lambda} v_{\mathbf{g}} \right) (pT_p) \right). \tag{29}$$

Denote $\frac{2}{\lambda} v_{\mathbf{g}} = \hat{p}.\Delta F_D$, where $\Delta F_D = \frac{1}{NT_p}$ is the Doppler frequency step; $\hat{p}$ is the unknown Doppler index at the moment of imaging; then the complex image function $\hat{a}_{\mathbf{g}} = \hat{a}_{\mathbf{g}}(\hat{p},k)$ in discrete space coordinates can be written as

$$\hat{a}_{\mathbf{g}}(\hat{p},k) = \sum_{p=1}^{N} s(p,k) \exp\left(j2\pi \frac{p\hat{p}}{N} \right). \tag{30}$$

The equation (30) stands for an IFT of $s(p,k)$ for each kth range resolution cell and can be considered as phase and/or motion compensation of first order.

Denote $a_1 = \frac{2}{\lambda} v_{\mathbf{g}}$, $a_2 = \frac{2\pi}{\lambda} a_{\mathbf{g}}$, $a_3 = \frac{2\pi}{3\lambda} h_{\mathbf{g}}$, then (28) can be rewritten as

$$\hat{a}_{\mathbf{g}} = \sum_{p=1}^{N} s(p,k) \exp\left(j[a_2(pT_p)^2 + a_3(pT_p)^3 + ...] \right) \exp\left(j2\pi a_1(pT_p) \right) \tag{31}$$

Denote $\Phi(p) = a_2(pT_p)^2 + ... + a_m(pT_p)^m$ as a phase correction and/or motion compensation function of higher order, then

$$\hat{a}_{\mathbf{g}}(\hat{p},k) = \sum_{p=1}^{N} \left[s(p,k) \exp\left(j\Phi(p) \right) \right] . \exp\left(j2\pi \frac{p\hat{p}}{N} \right). \tag{32}$$

where $\hat{a}_{\mathbf{g}}(\hat{p},k)$ denotes the complex azimuth image of the target, $\hat{p}$ denotes the unknown index of the azimuth space coordinate equal to the unknown Doppler index of the generic point scatterer from the target at the moment of imaging. The polynomial coefficients a_m , m = 2, 3, are calculated iteratively via applying image quality criterion, which will be discussed in subsections 4.4.

Eq. (32) can be interpreted as an ISAR image reconstruction procedure implemented through inverse Fourier transform (IFT) of a phase corrected ISAR signal into a complex azimuth image $\hat{a}_{\mathbf{g}}(\hat{p},k)$ for each kth range cell. In this sense the ISAR signal $s(p,k)$ can be referred to as a spatial frequency spectrum whereas $\hat{a}_{\mathbf{g}}(\hat{p},k)$ can be referred to as a spatial image function defined at the moment of imaging. Based on Eq. (32) two steps of image reconstruction algorithm can be outlined.

Step 1 Compensate the phases, induced by higher order radial movement, by multiplication of $s(p,k)$ with the exponential term $\exp[j\Phi(p)]$, i.e.

$$\hat{s}(p,k) = s(p,k)\exp[j\Phi(p)] \tag{33}$$

Step 2 Compensate the phases induced by first order radial displacement of generic points in the kth range cell by applying IFT (extract complex image), i.e.

$$\hat{a}_{\mathbf{g}}(\hat{p},k) = \sum_{p=1}^{N} \hat{s}(p,k).\exp\left(j2\pi \frac{p\hat{p}}{N} \right) \tag{34}$$

Complex image extraction can be implemented by inverse fast Fourier transform (IFFT). The algorithm can be implemented if the phase correction function $\Phi(p)$ is preliminary known.

Otherwise only IFT can be applied. Then non compensated radial acceleration and jerk of the target still remain and the image becomes blurred (unfocused). In order to obtain a focused image motion compensation of second, third and/or higher order has to be applied, that means coefficients of higher order terms in $\Phi(p)$ have to be determined. The definition and application of these terms in image reconstruction is named an autofocus procedure accomplished by an optimization step search algorithm (SSA) which will be discussed in subsection 4.4.

4. ISAR signal formation and imaging with a sequence of LFM waveforms

4.1 LFM waveform

Consider 3-D ISAR scenario (Fig. 6) and a target illuminated by sequence of LFM waveforms, each of which is described by

$$s(t) = A.\text{rect}\left(\frac{t}{T} \right)\exp\left[-j\left(\omega t + bt^2 \right) \right], \tag{35}$$

where $t = \tilde{t} - pT_p$ is the fast time and $\tilde{t} = t \bmod T_p$ is the slow time; p is the index of emitted pulse; T_p is the pulse repetition period; $\omega = 2\pi \frac{c}{\lambda}$ is the carrier angular frequency; $c = 3.10^8$ m/s is the speed of the light; λ is the wavelength of the signal; T is the timewidth of a LFM

waveform; $b = \frac{2\pi\Delta F}{T}$ is the LFM rate. The bandwidth $2\Delta F$ of the transmitted waveform provides the dimension of the range resolution cell, i.e. $\Delta R = c / 2\Delta F$.

4.2 LFM ISAR signal model

The deterministic component of the ISAR signal, reflected by the **g**th generic point scatterer has the form

$$s_{\mathbf{g}}(p,t) = a_{\mathbf{g}} \operatorname{rect}\frac{t - t_{\mathbf{g}}(p)}{T} \exp\left\{-j\left[\omega\left(t - t_{\mathbf{g}}(p)\right) + b\left(t - t_{\mathbf{g}}(p)\right)^2\right]\right\} \tag{36}$$

$$\operatorname{rect}\frac{t - t_{\mathbf{g}}(p)}{T} = \begin{cases} 1, 0 \le \dfrac{t - t_{\mathbf{g}}(p)}{T} < 1 \\ 0, \text{otherwise} \end{cases},$$

where $a_{\mathbf{g}}$ is the reflection coefficient of the **g**th generic point scatterer, a 3-D image function; $t_{\mathbf{g}}(p) = \frac{R_{\mathbf{g}}(p)}{c}$ is the round trip time delay of the signal from **g**th generic point scatterer; $R_{\mathbf{g}}(p) = \operatorname{mod}[\mathbf{R}_{\mathbf{g}}(p)]$, $t = [k_{\mathbf{g}\min}(p) + k - 1]\Delta T$ is the fast time, $k = \overline{1, K(p) + K}$ is the sample number of a LFM pulse; $K = T / \Delta T$ is the full number of samples of the LFM pulse, ΔT is the time duration of a LFM sample, $k_{\mathbf{g}\min}(p) = \left\lceil \frac{t_{\mathbf{g}\min}(p)}{\Delta T} \right\rceil$ is the number of the radar range cell where the signal, reflected by the nearest point scatterer of the target is detected, $t_{\mathbf{g}\min}(p) = \frac{2R_{\mathbf{g}\min}(p)}{c}$ is the minimal time delay of the SAR signal reflected from the nearest point scatterer of the target, $K(p) = k_{\mathbf{g}\max}(p) - k_{\mathbf{g}\min}(p)$ is the relative time dimension of the target; $k_{\mathbf{g}\max}(p) = \left\lceil \frac{t_{\mathbf{g}\max}(p)}{\Delta T} \right\rceil$ is the number of the radar range bin where the signal, reflected by farthest point scatterer of the target is detected; $t_{\mathbf{g}\max}(p) = \frac{2R_{\mathbf{g}\max}(p)}{c}$ is the maximum time delay of the SAR signal reflected from the farthest point scatterer of the target.

The ISAR signal in discrete form can be written as

$$s(p,k) = \sum_{\mathbf{g}\in\mathbf{G}} s_{\mathbf{g}}(p,k) = \sum_{\mathbf{g}\in\mathbf{G}} a_{\mathbf{g}} \operatorname{rect}\left[\frac{\hat{t}(p,k)}{T}\right] \exp\left\{-j\left[\omega\hat{t}(p,k) + b\left(\hat{t}(p,k)\right)^2\right]\right\} \tag{37}$$

$$\operatorname{rect}\left[\frac{\hat{t}_{\mathbf{g}}(p,k)}{T}\right] = \begin{cases} 1 \text{ if } 0 \le \dfrac{\hat{t}_{\mathbf{g}}(p,k)}{T} < 1, \\ 0 \text{ otherwise.} \end{cases}$$

where $\hat{t}_{\mathbf{g}}(p,k) = [k_{\mathbf{g}\min}(p) + k - 1]\Delta T - t_{\mathbf{g}}(p)$.

Demodulation of the ISAR signal return is performed by its multiplication by the complex conjugated emitted waveform, i.e.

$$\hat{s}(p,t)=\sum_{\mathbf{g}\in\mathbf{G}} a_{\mathbf{g}}\,\mathrm{rect}\frac{t-t_{\mathbf{g}}(p)}{T}\exp\left\{j\left[\omega\left(t-t_{\mathbf{g}}(p)\right)+b\left(t-t_{\mathbf{g}}(p)\right)^2\right]\right\}.\exp\left[-j\left(\omega t+bt^2\right)\right] \quad (38)$$

which yields

$$\hat{s}(p,t)=\sum_{\mathbf{g}\in\mathbf{G}} a_{\mathbf{g}}\,\mathrm{rect}\frac{t-t_{\mathbf{g}}(p)}{T}\exp\left\{-j\left[\left(\omega+2bt\right)t_{\mathbf{g}}(p)-bt_{\mathbf{g}}^2(p)\right]\right\}. \quad (39)$$

Denote the current angular frequency of emitted LFM pulse as $\omega(t)=\omega+2bt$, which in discrete form can be expressed as $\omega_k=\omega+2b(k-1)\Delta T$, where ω is the carrier angular frequency, and b is the chirp rate, k is the LFM sample number, ΔT is the time length of the sample, then Eq. (39) can be rewritten as

$$\hat{s}(p,t)=\sum_{\mathbf{g}\in\mathbf{G}} a_{\mathbf{g}}\,\mathrm{rect}\frac{t-\dfrac{R_{\mathbf{g}}(p)}{c}}{T}\exp\left[-j\left(2\omega(t)\frac{R_{\mathbf{g}}(p)}{c}-b\left(\frac{2R_{\mathbf{g}}(p)}{c}\right)^2\right)\right], \quad (40)$$

which in discrete form can be expressed as

$$\hat{s}(p,k)=\sum_{\mathbf{g}\in\mathbf{G}} a_{\mathbf{g}}\,\mathrm{rect}\frac{\hat{t}_{\mathbf{g}}(p,k)}{T}\exp\left[-j\left(2\omega_k\frac{R_{\mathbf{g}}(p)}{c}-b\left(\frac{2R_{\mathbf{g}}(p)}{c}\right)^2\right)\right]. \quad (41)$$

Eq. (41) can be interpreted as a spatial transform of the 3-D image function $a_{\mathbf{g}}$ into 2-D ISAR signal plane $\hat{s}(p,k)$ by the finite transformation operator, the exponential term

$$\exp\left[-j\left(2\omega_k\frac{R_{\mathbf{g}}(p)}{c}-b\left(\frac{2R_{\mathbf{g}}(p)}{c}\right)^2\right)\right]. \quad (42)$$

Formally the 3-D image function $a_{\mathbf{g}}$ should be extracted from 2-D ISAR signal plane by the inverse spatial transform but due to theoretical limitation based on the number of measurement parameters only a 2-D image function may be extracted, i.e.

$$\hat{a}_{\mathbf{g}\in\mathbf{G}}=\sum_{p=1}^{N}\sum_{k=1}^{K(p)+K}\hat{s}(p,k).\exp\left[j\left(2\omega_k\frac{R_{\mathbf{g}}(p)}{c}-b\left(\frac{2R_{\mathbf{g}}(p)}{c}\right)^2\right)\right]. \quad (43)$$

Extraction of the image function is a procedure of complete phase compensation of the signals reflected by all point scatterers from the object that means total compensation of target movement during CPI. The argument of the exponential term (43), $\left(2\omega_k\frac{R_{\mathbf{g}}(p)}{c}-b\left(\frac{2R_{\mathbf{g}}(p)}{c}\right)^2\right)$ is a complex function infinitely differentiable in a neighborhood

of the moment of imaging that allows 2-D Taylor expansion on range and azimuth direction to be applied, i.e. the following polynomial of higher order to be defined

$$\left(2\omega_k \frac{R_{\mathbf{g}}(p)}{c} - b\left(\frac{2R_{\mathbf{g}}(p)}{c}\right)^2\right) = a_0 + a_1.(pT_p) + a_2.(pT_p)^2 + ... + a_m(pT_p)^m$$
$$+b_1.(k\Delta T) + b_2.(k\Delta T)^2 + ... + b_m(k\Delta T)^m + c_2(pT_p)(k\Delta T) + ... \tag{44}$$

The constant terms a_0 has noting to do with phase correction and can be neglected. The linear terms $a_1.(pT_p)$ and $b_1.(k\Delta T)$ are redefined as $a_1(pT_p) = 2\pi\frac{p\hat{p}}{N}$ and $b_1(k\Delta T) = 2\pi\frac{k\hat{k}}{\hat{K}}$, where $\hat{k} = \hat{k}(\mathbf{g}), \hat{p} = \hat{p}(\mathbf{g})$ denote the new unknown range and cross-range space coordinates of the **g**th generic point at the instant of imaging, $\hat{K} = K + K(p)$ denotes the number of range cells for each emitted pulse. The sum of higher order terms is signified as

$$\Phi(p,k) = a_2.(pT_p)^2 + ... + a_m(pT_p)^m + b_2.(k\Delta T)^2 + ... + b_m(k\Delta T)^m + c_2(pT_p)(k\Delta T) + ... \tag{45}$$

then

$$\left(2\omega_k \frac{R_{\mathbf{g}}(p)}{c} - b\left(\frac{2R_{\mathbf{g}}(p)}{c}\right)^2\right) = 2\pi\frac{p\hat{p}}{N} + 2\pi\frac{k\hat{k}}{K} + \Phi(p,k)\,. \tag{46}$$

Substitute (46) in (43), then

$$\hat{a}_{\mathbf{g}}(\hat{p},\hat{k}) = \sum_{p=1}^{N}\sum_{k=1}^{\hat{K}} \hat{s}(p,k)\exp\left[j\left(\Phi(k,p) + 2\pi\frac{p\hat{p}}{N} + 2\pi\frac{k\hat{k}}{K}\right)\right], \tag{47}$$

where $\hat{p} = \overline{1,N}$, $\hat{k} = \overline{1,K(p)+K}$.

Eq. (47) can be rewritten as

$$\hat{a}_{\mathbf{g}}(\hat{p},\hat{k}) = \sum_{p=1}^{N}\left[\sum_{k=1}^{\hat{K}} \hat{s}(p,k).\exp\left[j\Phi(k,p)\right].\exp\left(j2\pi\frac{k\hat{k}}{\hat{K}}\right)\right]\exp\left(j2\pi\frac{p\hat{p}}{N}\right). \tag{48}$$

Eq. (48) can be considered as an image reconstruction computational procedure, which does reveal the 2-D discrete complex image function $\hat{a}_{\mathbf{g}}(\hat{p},\hat{k})$.

4.3 LFM ISAR image reconstruction algorithm

Based on the previous analysis the following image reconstruction steps can be defined.

Step 1 Compensate phase terms of higher order by multiplication of complex matrix $\hat{s}(p,k)$ by a complex exponential function $\exp\left[j\Phi(p,k)\right]$, i.e.

$$\tilde{s}(p,k) = \hat{s}(p,k).\exp\left[j\Phi(p,k)\right] \tag{49}$$

Step 2 Range compress $\tilde{s}(p,k)$ by discrete IFT, i.e.

$$\tilde{s}(p,\hat{k}) = \frac{1}{\hat{K}}\sum_{k=1}^{\hat{K}} \tilde{s}(p,k).\exp\left(j2\pi\frac{k\hat{k}}{\hat{K}}\right). \tag{50}$$

Step 3 Azimuth compress $\tilde{s}(p,\hat{k})$, i.e. extract a complex image by IFT

$$a_{\mathbf{g}}(\hat{p},\hat{k}) = \frac{1}{N}\sum_{p=1}^{N} \tilde{s}(p,\hat{k}).\exp\left(j2\pi\frac{p\hat{p}}{N}\right). \tag{51}$$

Step 4 Compute the module of the complex image by

$$\left|a_{\mathbf{g}}(\hat{p},\hat{k})\right| = \left|\frac{1}{N}\sum_{p=1}^{N} \tilde{s}(p,\hat{k}).\exp\left(j2\pi\frac{p\hat{p}}{N}\right)\right|. \tag{52}$$

The aforementioned algorithm is feasible if the phase correction function $\Phi(p,k)$ is a priory known. Otherwise, a focused image is impossible to extract. In this case taking into account the linear property of computational operations in (48) the image extraction algorithm may start with 2-D IFT (range and cross range compression) of the demodulated ISAR signal, the complex matrix $\hat{s}(p,k)$, i.e.

$$a_{\mathbf{g}}(\hat{p},\hat{k}) = \sum_{p=1}^{N}\left[\sum_{k=1}^{\hat{K}} \hat{s}(p,k).\exp\left(j2\pi\frac{k\hat{k}}{\hat{K}}\right)\right]\exp\left(j2\pi\frac{p\hat{p}}{N}\right). \tag{53}$$

It is worth noting that 2-D IFT are interpreted as a spatial correlation of the complex frequency spectrum, $\hat{s}(p,k)$ with the exponential terms $\exp\left(j2\pi\frac{k\hat{k}}{\hat{K}}\right)$ and $\exp\left(j2\pi\frac{p\hat{p}}{N}\right)$ that reveal unknown range, $\hat{k}$ and cross range, $\hat{p}$ space coordinates of a 2-D image function $a_{\mathbf{g}}(\hat{p},\hat{k})$ in the area of all possible values $\hat{p} = \overline{1,N}$ and $\hat{k} = \overline{1,K(p)+K}$.

4.4 Autofocusing phase correction by image entropy minimization

If the image obtained by only range (50) and azimuth (51) compression is blurred a higher order phase correction has to be applied, i.e. to perform $\tilde{s}(k,p) = \hat{s}(k,p).\exp\left[j\Phi(p)\right]$. The phase correction or motion compensation of higher order is an autofocus procedure. It requires determination of coefficients $a_2 \ldots a_m$, $b_2 \ldots b_m$ and c_2 of the polynomial (45). The computational load is reduced if $\Phi(p,k) = \Phi(p)$ for each k, i.e. (45) is limited to

$$\Phi(p) = a_2.(pT_p)^2 + \ldots + a_m(pT_p)^m \tag{54}$$

An iterative SSA is applied to find out optimal values of the coefficients using entropy as a cost function to evaluate the quality of the image. At first step a_2 is calculated, at second - a_3, etc. The exact value of each coefficient a_m, $m = 2,3,\ldots$ is computed iteratively, starting from

$a_m = 0$ and increasing by $\Delta a_m = 0.01$ in case the image quality gets better. If the image quality does not improve or gets worse go to computation of the next coefficient a_{m+1} or stop the procedure. In practice the quadratic term has a major impact on the phase correction process.

Let $\Phi_s(p)$ be a phase correction function, defined at the sth iteration, and then the phase correction is accomplished by

$$\tilde{s}_s(p,k) = \hat{s}(p,k)\exp(-j\Phi_s(p)). \tag{55}$$

After current phase correction and image extraction by range and cross-range (azimuth) compression, calculate a power normalized image as

$$I_s(\hat{p},\hat{k}) = \frac{\left|a_{\mathbf{g},s}(\hat{p},\hat{k})\right|^2}{\sum_{p=1}^{N}\sum_{k=1}^{\hat{K}}\left|a_{\mathbf{g},s}(\hat{p},\hat{k})\right|^2}. \tag{56}$$

Calculate entropy of the normalized ISAR image

$$H_s = -\sum_{p=1}^{N}\sum_{k=1}^{\hat{K}} I_s(\hat{p},\hat{k})\ln[I_s(\hat{p},\hat{k})]. \tag{57}$$

The estimate of the optimal values of coefficients corresponds to the minimum of the entropy image cost function, i.e.

$$\hat{a}_m = \arg\min_{a_m}\left\{H_s[I_s(\hat{p},\hat{k})]\right\}. \tag{58}$$

The procedure is repeated until the global minimum value of the entropy H_s is acquired.

4.5 Numerical experiment

To verify the properties of the LFM ISAR signal model and to prove the correctness of the image reconstruction algorithm a numerical experiment is carried out. Assume the target, Mig-35, detected in 3-D coordinate system $O'XYZ$ is moving rectilinearly in a coordinate system $Oxyz$. Kinematical parameters: velocity $V = 400$ m/s; guiding angles $\alpha = 0.92\pi$; $\beta = -0.5\pi$; $\gamma = 0.42\pi$, coordinates of the mass-center at the moment ($p = N/2$): $x_{00'}(0) = 36{,}3.10^3$ m; $y_{00'}(0) = 71{,}3.10^3$ m; $z_{00'}(0) = 5.10^3$ m; reference coordinates: $x_0(0) = 10$ m; $y_0(0) = 5.10^4$ m; $z_0(0) = 2.10^3$ m. LFM emitted pulse: wavelength $\lambda = 3.10^{-2}$ m; pulse repetition period $T_p = 1.32.10^{-2}$ s, LFM pulse timewidth $T = 10^{-6}$ s; number of LFM samples $K = 300$; timewidth of LFM sample $\Delta T = 0.33.10^{-8}$ s; bandwidth $\Delta F = 1.5.10^8$ Hz, LFM rate $b = 3.10^{14}$ s^{-2}; number of emitted pulses during CPI $N = 500$. Dimensions of the grid cell: $\Delta X = \Delta Y = \Delta Z = 0.5$ m; reference points on grid axes X, Y, Z, $i = \overline{1,64}$, $j = \overline{1,64}$ $k = \overline{1,10}$. Target intensities $a_{ijk} = 0.01$, out of target intensities $a_{ijk} = 0.001$.

The complex spatial frequency spectrum and 2-D space image function are presented in Figs. 7 and 8, respectively. The entropy and final focused image of Mig-35 are illustrated in Figs. 9 and 10, respectively.

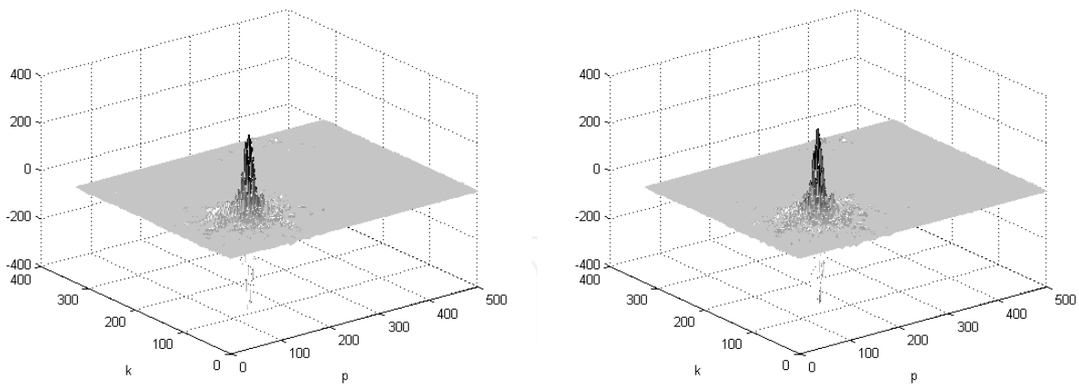

(a) Imaginary part of the ISAR signal (b) Real part of the ISAR signal

Fig. 7. Complex ISAR signal - complex spatial frequency spectrum.

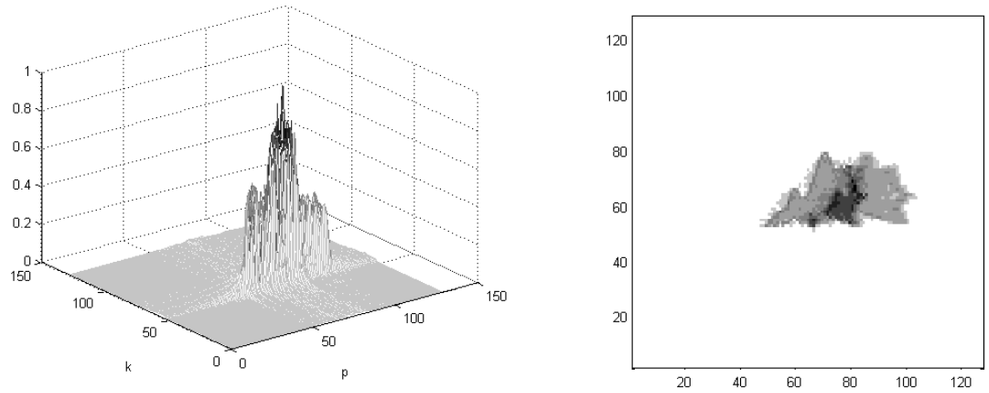

(a) Module of the 2-D space image function (b) Unfocused image of Mig-35

Fig. 8. 2-D isometric space image function and 2-D unfocused image of Mig-35 after azimuth compression by second IFT.

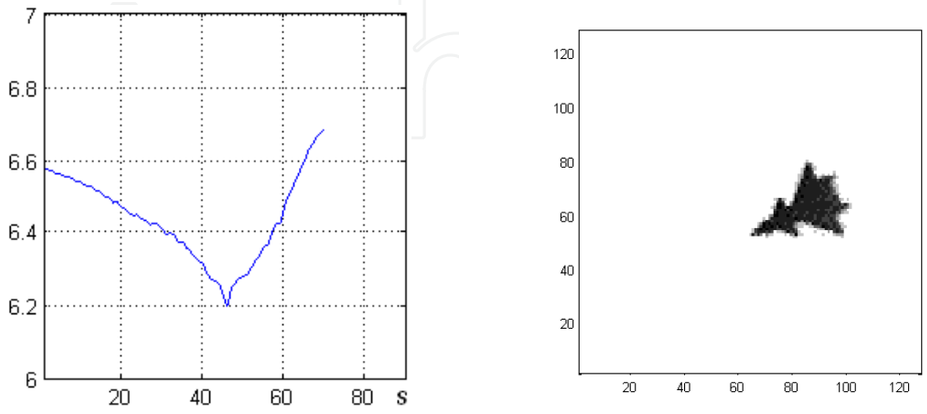

(a) Evolution of the image entropy (b) Final focused image of Mig-35

Fig. 9. Image entropy and final focused image of Mig-35 by step 47 and minimal entropy 6.2.

5. ISAR signal formation and imaging with a sequence of PCM waveforms

5.1 PCM waveform

Consider 3-D ISAR scenario (Fig. 6) and a target a sequence of phase-code modulated (PCM) pulse trains (bursts). Each PCM pulse train is described by

$$s(t) = A\mathbf{rect}\frac{t}{T}\exp\left\{-j\left[\omega t + \pi b(t) + \varphi_0\right]\right\}, \tag{59}$$

where $t = \tilde{t} - pT_p$ is the fast time and $\tilde{t} = t \bmod T_p$ is the slow time; p is the index of the emitted pulse train; T_p is the burst repetition period; φ_0 is the initial phase of a PCM pulse, $k = \overline{1,K}$ is the index of the PCM segment, $K = T/\Delta T$ is the full number of PCM segments; T is the time duration of the phase-code modulated pulse train, ΔT is the timewidth the phase segment, $b(t) \in \{0,1\}$ is the binary parameter of the PCM train.

5.2 PCM ISAR signal model

Deterministic component of the ISAR signal return reflected by the **g**th generic point scatterer if $\varphi_0 = 0$ is defined by

$$s_{\mathbf{g}}(p,t) = a_{\mathbf{g}}\,\mathrm{rect}\frac{t - t_{\mathbf{g}}(p)}{T}\exp\left\{-j\left[\omega(t - t_{\mathbf{g}}(p)) + \pi b(t)\right]\right\}, \tag{60}$$

$$\mathrm{rect}\frac{t - t_{\mathbf{g}}(p)}{T} = \begin{cases} 1, & \text{if } 0 \le \dfrac{t - t_{\mathbf{g}}(p)}{T} < 1; \\ 0, & \text{otherwise.} \end{cases}$$

The deterministic component of the ISAR signal return reflected from the target for every p th pulse train is described by

$$s(p,t) = \sum_{\mathbf{g}\in\mathbf{G}} a_{\mathbf{g}}\,\mathrm{rect}\frac{t - t_{\mathbf{g}}(p)}{T}\exp\left\{-j\left[\omega(t - t_{\mathbf{g}}(p)) + \pi b(t)\right]\right\}. \tag{61}$$

Eq. (61) is a weighted complex series of finite base functions, ISAR signals from all generic points. It can be regarded as an asymmetric complex transform of the 3-D image function $a_{\mathbf{g}\in\mathbf{G}}$, into a 2-D signal plane $\hat{s}(k,p)$. Computing $\mathrm{rect}[t - t_{\mathbf{g}}(p)/T]$ time delays $t_{\mathbf{g}}(p)$ are arranged in ascending order. An index $\hat{k}$ different from this order is introduced i.e. $t_{\mathbf{g}}^{\hat{k}}(p)$. Denote $\hat{t}_{\mathbf{g}}^{\hat{k}}(p) = (k_{\mathbf{g}\min}(p) + k - 1)\Delta T - t_{\mathbf{g}}^{\hat{k}}(p)$, then Eq. (60) in discrete form can be written as

$$s(p,k) = \sum_{\mathbf{g}\in\mathbf{G}} a_{\mathbf{g}}\,\mathrm{rect}\frac{\hat{t}_{\mathbf{g}}^{\hat{k}}(p)}{T}.\exp\left\{-j\left[\omega\hat{t}_{\mathbf{g}}^{\hat{k}}(p) + \pi b(k - \hat{k} + 1)\Delta T\right]\right\}, \tag{62}$$

$$\mathrm{rect}\frac{\hat{t}_{\mathbf{g}}^{\hat{k}}(p)}{T} = \begin{cases} 1, & \text{if } 0 \le \dfrac{\hat{t}_{\mathbf{g}}^{\hat{k}}(p)}{T} < 1 \\ 0, & \text{otherwise} \end{cases}.$$

where $\hat{k}$ stands for a current range number k for which $\text{rect}[\hat{t}_{\mathbf{g}}^{\hat{k}}(p)/T]$ yields 1 first time. It is possible for many time delays, $t_{\mathbf{g}}(p)$ the index $\hat{k}$ to have one and the same value. The index $\hat{k}$ is considered as a space discrete range coordinate of a **g**th generic point at the moment of imaging.

5.3 PCM ISAR image reconstruction procedure

Based on the phase demodulated ISAR signal

$$\hat{s}(p,k)=\sum_{\mathbf{g}\in\mathbf{G}} a_{\mathbf{g}}\,\text{rect}\frac{\hat{t}_{\mathbf{g}}^{\hat{k}}(p)}{T}\exp\left\{-j\left[\omega(k_{\mathbf{g}\min}(p)\Delta T-t_{\mathbf{g}}^{\hat{k}}(p))+\pi b((k-\hat{k}+1)\Delta T)\right]\right\}. \tag{63}$$

formally the 3-D image function $a_{\mathbf{g}}$ should be extracted from 2-D ISAR signal plane by the inverse spatial transform but due to theoretical limitation based on the number of measurement parameters only a 2-D image function may by determined, i.e.

$$\hat{a}_{\mathbf{g}}=\sum_{p=1}^{N}\sum_{k=\hat{k}}^{\hat{k}+K} s(p,k)\exp\left\{j\left[\omega(k_{\mathbf{g}\min}(p)\Delta T-t_{\mathbf{g}}^{\hat{k}}(p))+\pi b((k-\hat{k}+1)\Delta T)\right]\right\}, \tag{64}$$

Eq. (64) can be rewritten as

$$\hat{a}_{\mathbf{g}}=\sum_{p=1}^{N}\sum_{k=\hat{k}}^{\hat{k}+K}\left[\hat{s}(p,k)\exp[j\pi b(k-\hat{k}+1)\Delta T]\right].\exp\left\{j\omega\left[k_{\mathbf{g}\min}(p)\Delta T-t_{\mathbf{g}}^{\hat{k}}(p)\right]\right\}. \tag{65}$$

Taylor expansion of the phase term $\left[t_{ijk\min}(p)-t_{ijk}^{\hat{k}}(p)\right]$ can be presented as a polynomial function of higher order, i.e.

$$\left[k_{\mathbf{g}\min}(p)-t_{ijk}^{\hat{k}}(p)\right]=a_0+a_1(pT_p)+a_2(pT_p)^2+\ldots+a_m(pT_p)^m. \tag{66}$$

The linear term $a_1(pT_p)$ is reduced to $\frac{2\pi}{N}\hat{p}.p$ and considered as a Fourier operator, $\hat{p}$ is the discrete unknown coordinate of the gth generic point scatterer placed in the kth range cell, N is the number of emitted PCM trains during CPI. The constant term has nothing to do with the image reconstruction and is removed. The rest sum of the terms in (66) are denoted as

$$\Phi(p)=a_2(pT_p)^2+\ldots+a_m(pT_p)^m, \tag{67}$$

then (65) can expressed as

$$\hat{a}_{\mathbf{g}}(\hat{p},\hat{k})=\sum_{p=1}^{N}\sum_{k=\hat{k}}^{\hat{k}+K}\left\{\hat{s}(p,k)\exp\left[j\pi b(k-\hat{k}+1)\Delta T\right]\right\}\exp\left\{j\left[\frac{2\pi}{N}p\hat{p}+\Phi(p)\right]\right\}, \tag{68}$$

Based on the linearity of the operations (68) can be rewritten as

$$\hat{a}_{\mathbf{g}}(\hat{p},\hat{k})=\sum_{p=1}^{N}\left\{\sum_{k=\hat{k}}^{\hat{k}+K}\left[\hat{s}(p,k).\exp(j\Phi(p)\right].\exp[j\pi b(k-\hat{k}+1)\Delta T)]\right\}\exp\left\{j\left[\frac{2\pi}{N}\hat{p}p\right]\right\}. \tag{69}$$

Accordingly, the image extraction algorithm can be outlined as follows.

Step 1 Phase correction by multiplication of the phase demodulated ISAR signal with an exponential phase correction function, i.e.

$$\tilde{s}(p,k) = \hat{s}(p,k).\exp[j\Phi(p)]. \tag{70}$$

Step 2 Range compression is by correlating of the phase corrected ISAR signal $\tilde{s}(p,k)$ with reference function, complex conjugated of the transmitted PCM signal $\exp[j\pi b(k-\hat{k}+1)\Delta T]$, i.e.

$$\tilde{s}(\hat{p},\hat{k}) = \sum_{k=\hat{k}}^{\hat{k}+K} \tilde{s}(p,k)\exp[j\pi b(k-\hat{k}+1)\Delta T], \tag{71}$$

where $p = \overline{1,N}$, $\hat{k} = \overline{1,K(p)}$.

Step 3 Azimuth compression and complex image extraction by Fourier transform of the range compressed ISAR data, i.e.

$$\hat{a}_{\mathbf{g}}(\hat{p},\hat{k}) = \sum_{p=1}^{N} \tilde{s}(p,\hat{k})\exp\left\{j\left[\frac{2\pi}{N}\hat{p}p\right]\right\}. \tag{72}$$

Then the module of the target image can be calculated by

$$\left|\hat{a}_{\mathbf{g}}(\hat{p},\hat{k})\right| = \left|\sum_{p=\overline{1,N}} \tilde{s}(p,\hat{k})\exp\left\{j\left[\frac{2\pi}{N}\hat{p}p\right]\right\}\right|. \tag{73}$$

The aforementioned algorithm is feasible if the phase correction function $\Phi(p,k)$ is a priory known. Otherwise, a focused image is impossible to extract. In this case taking into account the linear property of computational operations in (68) the image extraction algorithm may start with correlation along range coordinate (range compression) and Fourier transform along cross range coordinate (range compression) of the demodulated ISAR signal, the complex matrix $\hat{s}(p,k)$, i.e.

$$\hat{a}_{\mathbf{g}}(\hat{p},\hat{k}) = \sum_{p=1}^{N}\left\{\sum_{k=\hat{k}}^{\hat{k}+K} \hat{s}(p,k).\exp[j\pi b((k-\hat{k}+1)\Delta T)]\right\}\exp\left\{j\left[\frac{2\pi}{N}\hat{p}p\right]\right\}. \tag{74}$$

If the image obtained by only range (71) and azimuth (72) compression is blurred a higher order phase correction algorithm has to be applied. It requires determination of coefficients $a_2 \ldots a_m$ in polynomial (67) using a phase correction SSA described in 4.4.

5.4 Numerical experiment

A numerical experiment is carried out to verify the properties of the PCM ISAR signal model and to prove the correctness of the image reconstruction algorithm. It is assumed that the target, helicopter is detected in a coordinate system $O'XYZ$ and illuminated by Barker's

PCM burst and moving rectilinearly in a coordinate system $Oxyz$. Kinematic parameters: velocity module $V = 25$ m/s; velocity guiding angles $\alpha = 0$, $\beta = 0.5\pi$, $\gamma = 0.5\pi$; coordinates of the mass-centre: $x_{00'}(0) = 0$ m, $y_{00'}(0) = 5.10^4$ m, $z_{00'} = 3.10^3$ m. Barker's PCM binary function $b(t)$: $b(t) = 0$ if $t = (\overline{1,5},\overline{8,9},11,13)\Delta T$, and $b(t) = 1$ if $t = (\overline{6,7},10,12)\Delta T$; wavelength $\lambda = 3.10^{-2}$ m; burst repetition period $T_p = 5.10^{-3}$ s; PCM sample timewidth $\Delta T = 3.3.10^{-9}$ s; number of burst samples $K = 13$; sample index $k = \overline{1,13}$; PCM burst timewidth $T = 42.9.10^{-9}$ s; number of bursts emitted during CPI $N = 500$. Grid's cell dimensions $\Delta X = \Delta Y = \Delta Z = 0.5$ m. Reference points on axes X,Y,Z $i = j = \overline{1,100}$ and $k = \overline{1,40}$, respectively. Isotropic point scatterers are placed at each node of the regular grid. Target's intensities $a_{ijk} = 0.01$, out of target's intensities $a_{ijk} = 0.001$.

The real and imaginary part of the complex Barker's PCM ISAR signal is presented in Fig. 10, the final image – 2-D space image function - in Fig. 11, and entropy evolution in Fig. 12.

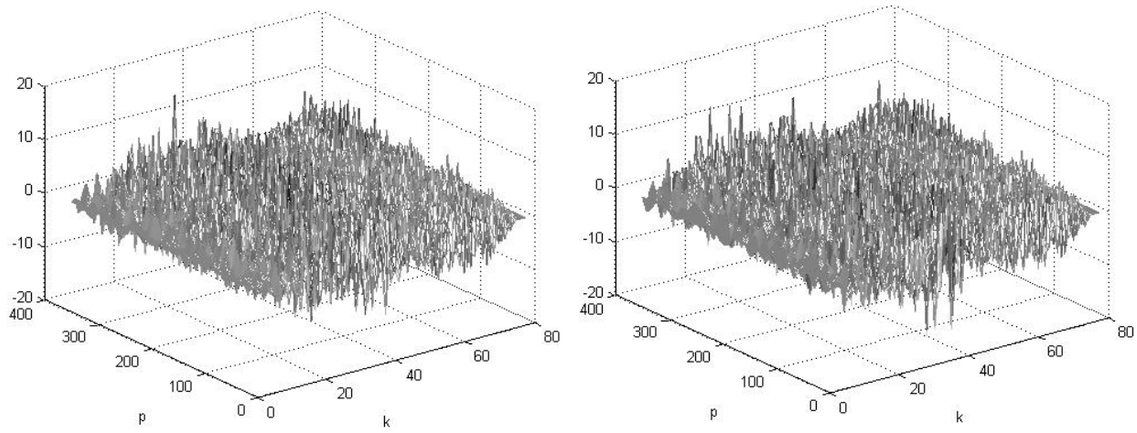

(a) Real part of ISAR signal (b) Imaginary part of ISAR signal

Fig. 10. Complex Barker's PCM ISAR signal as a complex spatial frequency spectrum.

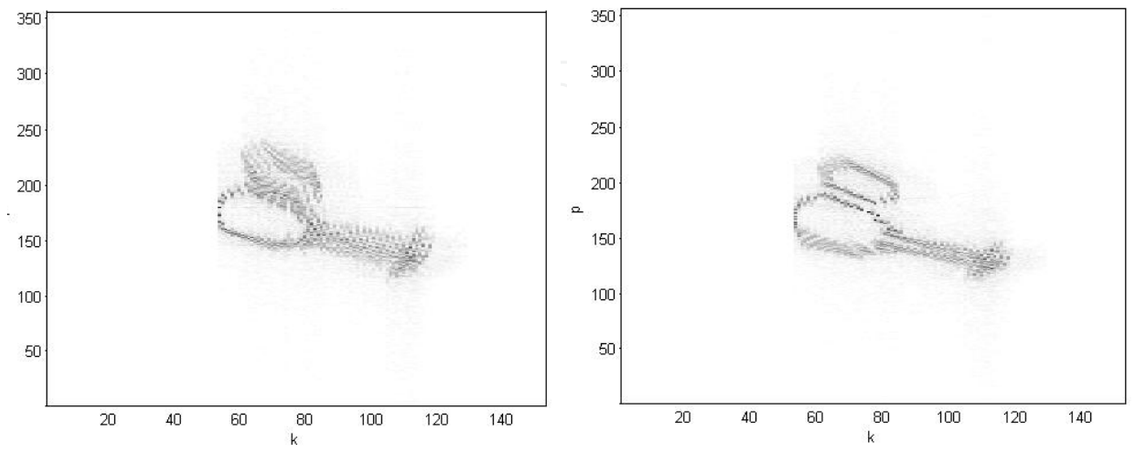

(a) Unfocused ISAR image (b) Focused ISAR image

Fig. 11. Final image – 2-D space image function (pseudo color maps).

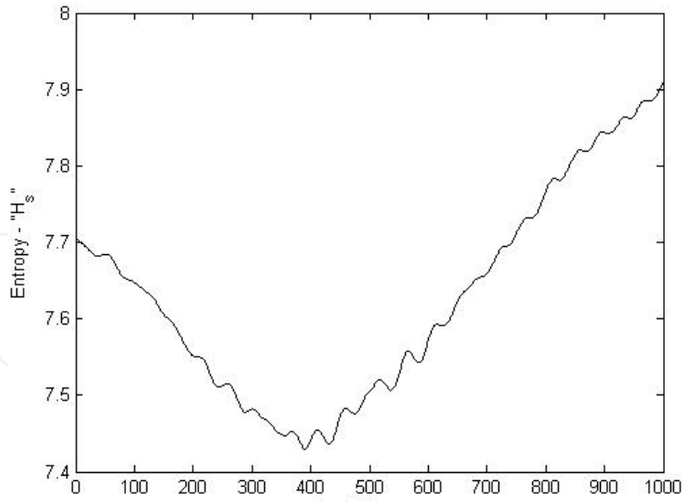

Fig. 12. Entropy evolution: $H_{\min} = 7,43$ by optimal vale of $a_2 = 390$.

6. Conclusion

In the present chapter a mathematical description and original interpretation of ISAR signal formation and imaging has been suggested. It has been illustrated that both of these operations can be interpreted as direct and inverse spatial complex transforms, respectively. It has been proven that the image extraction is a threefold procedure; including phase correction, range compression performed by IFT in case LFM waveforms and by cross-correlation in case PCM waveforms, and azimuth compression performed by IFT in both cases. It has been underlined that the image reconstruction is a procedure of total motion compensation, i.e. compensation of all phases induced by the target motion. Only phases proportional to the distances from ISAR to all point scatterers on the target at the moment of their imaging still remain. These phases define a complex character of the ISAR image. The drawback of the proposed higher motion compensation algorithm is the existence of multiple local minimums in entropy evolution in case the target is fast maneuvering. In order to find out a global minimum in the entropy and optimal values of the polynomial coefficients the computation process has to be enlarged in wide interval of their variation. The subject of the future research is the exploration of the image reconstruction algorithm with higher order terms and cross-terms of the phase correction polynomial while the target exhibits complicated movement.

7. Acknowledgement

This chapter is supported by NATO Science for Peace and Security (SPS) Programme: NATO: ESP. EAP. CLG 983876.

8. References

Li, J.; Wu, R.; Chen, V. (2001). Robust autofocus algorithm for ISAR imaging of moving targets, *IEEE Transactions on Aerospace and Electronic Systems*, Vol. 37, No 3, (July 2001), pp. 1056-1069, ISSN 0018-9251

Berizzi, F.; Dalle Mese, E. & Martorella, M. (2002). Performance analysis of a contrast-based ISAR autofocusing algorithm. *Proceedings of 2002 IEEE Radar Conference*, pp. 200-205, ISBN 0-7803-7357-X, Long Beach, CA, USA, Apr. 22-25, 2002

Martorella, M.; Haywood, B.; Berizzi, F. & Dalle Mese, E. (2003). Performance analysis of an ISAR contrast-based autofocusing algorithm using real data. *Proceedings of 2003 IEEE Radar Conference*, pp. 30-35, ISBN 0-7803-7870-9, Adelaide, SA, Australia, Sept. 3-5, 2003

Berizzi, F.; Martorella, M.; Haywood, B. M.; Dalle Mese, E. &Bruscoli, S. (2004). A survey on ISAR autofocusing techniques. *Proceedings of IEEE ICIP 2004*, Singapore, Oct. 24-27, 2004

Chen, C. & Andrews, H.C. (1980). Target motion induced radar imaging. *IEEE Transactions on Aerospace and Electronic Systems*, Vol. 16, (January 1980), pp. 2-14, ISSN 0018-9251

Wu, H.; Delisle, G. Y. & Fang, D. G. (1995). Translational motion compensation in ISAR image processing. *IEEE Transactions on Image Processing*, Vol. 4, No 11, (November 1995), pp. 1561-1571, ISSN 0018-9251

Xi, L.; Guosui, L. & Ni, J. (1999). Autofocusing of ISAR images based on entropy minimization, *IEEE Transactions on Aerospace and Electronic Systems*, Vol. 35, No 4, (October 1999), pp. 1240-1252, ISSN 0018-9251

Martorella M. & Berizzi, F. (2005). Time windowing for highly focused ISAR image reconstruction," *IEEE Transactions on Aerospace and Electronic Systems,* Vol 41, No 3, (July 2005), pp. 992-1006, ISSN 1729-8806

Chen, V. & Quint, S. (1998). Joint time-frequency transform for radar range Doppler imaging. *IEEE Transactions on Aerospace and Electronic Systems*, Vol. 34, No 2, (April 1998) pp. 486-499, ISSN 0018-9251

Qian, S. & Chen, V. (1998). ISAR motion compensation via adaptive joint time-frequency technique, *IEEE Transactions on Aerospace and Electronic Systems*, Vol. 34, No 2, pp. 670-677, (April 1999), ISSN 0018-9251

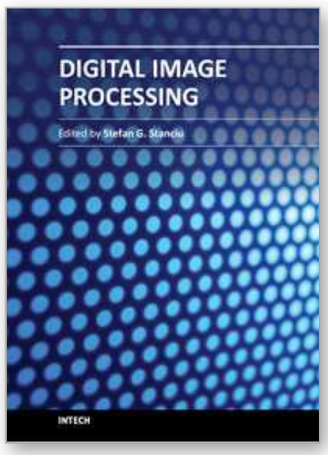

Digital Image Processing

Edited by Dr. Stefan G. Stanciu

ISBN 978-953-307-801-4
Hard cover, 200 pages
Publisher InTech
Published online 11, January, 2012
Published in print edition January, 2012

This book presents several recent advances that are related or fall under the umbrella of 'digital image processing', with the purpose of providing an insight into the possibilities offered by digital image processing algorithms in various fields. The presented mathematical algorithms are accompanied by graphical representations and illustrative examples for an enhanced readability. The chapters are written in a manner that allows even a reader with basic experience and knowledge in the digital image processing field to properly understand the presented algorithms. Concurrently, the structure of the information in this book is such that fellow scientists will be able to use it to push the development of the presented subjects even further.

How to reference

In order to correctly reference this scholarly work, feel free to copy and paste the following:

Andon Lazarov (2012). ISAR Signal Formation and Image Reconstruction as Complex Spatial Transforms, Digital Image Processing, Dr. Stefan G. Stanciu (Ed.), ISBN: 978-953-307-801-4, InTech, Available from: http://www.intechopen.com/books/digital-image-processing/isar-signal-formation-and-image-reconstruction-as-complex-spatial-transforms

INTECH
open science | open minds

InTech Europe
University Campus STeP Ri
Slavka Krautzeka 83/A
51000 Rijeka, Croatia
Phone: +385 (51) 770 447
Fax: +385 (51) 686 166
www.intechopen.com

InTech China
Unit 405, Office Block, Hotel Equatorial Shanghai
No.65, Yan An Road (West), Shanghai, 200040, China
中国上海市延安西路65号上海国际贵都大饭店办公楼405单元
Phone: +86-21-62489820
Fax: +86-21-62489821

IntechOpen